Nanoscale

Accepted Manuscript

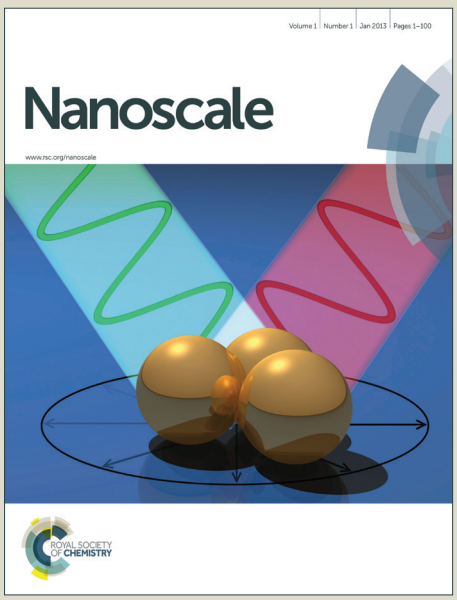

ROYAL SOCIETY OF CHEMISTRY

www.rsc.org/nanoscale

Nanoscale

ARTICLE

Nitrogen-Doped Graphene Networks Supported Copper Nanoparticles Encapsulated with Graphene Shells for Surface-Enhanced Raman Scattering

Received 00th January 20xx,
Accepted 00th January 20xx

DOI: 10.1039/x0xx00000x

www.rsc.org/

Xiang Zhang,[a] Chunsheng Shi,[a] Enzuo Liu,[a,b] Jiajun Li,[a] Naiqin Zhao, *[a,b] and Chunnian He *[a,b]

In this study, we demonstrated a nitrogen-doped graphene networks supported few-layer graphene shells encapsulated C nanoparticles (NPs) (Cu@G-NGNs) as a sensing platform, which were constructed by a simple and scalable in-situ chemic vapor deposition (CVD) technique with the assistance of a template of three-dimensional (3D) NaCl self-assembl Compared with pure Cu NPs and graphene decorated Cu NPs, the graphene shells can strengthen the plasmonic coup between graphene and Cu, thereby contributing to an obvious improvement in local electromagnetic field that was validated by Finite Element Numerical simulations, while the 3D nitrogen-doped graphene walls with large surface area facil molecules adsorption and the doped nitrogen atoms embedded in the graphene lattice can reduce the surface energy of the system. With these merits, the good surface enhanced Raman spectroscopy (SERS) activity of 3D Cu@G-NGNs pair film on glass was demonstrated using rhodamine 6G and crystal violet as model analyte, exhibiting a satisfactory sensibilit reproducibility and stability. As far as we know, this is the first report on the in-situ synthesis of nitrogen-doped graphene/copper nanocomposites and this facile and low-cost Cu-based strategy tends to be a good supplement to the A and Au based substrates for SERS applications.

Introduction

Surface-enhanced Raman scattering (SERS) is a powerful analytic method to identify and detect trace amount of molecules.[1] Metallic substrates based on nano-sized particles (NPs) of Ag, Au, Cu, etc. were found with strong SERS enhancement due to that the surface-plasmon resonance (SPR) of these free-electron metals can be effectively excited in the visible and/or near-IR ranges. Among them, Cu is one of the most promising substrate materials considering the advantages of low cost, strong adsorbability with organic molecules as well as simple and environmental friendly preparation process.[2,3] However, compared with Ag and Au, which are the focused noble metal SERS substrate of quantities of papers, Cu NPs have attracted fewer attentions because of their high activity in air and insignificant SERS enhancement.[4,5] Recently, some researches showed that, with delicate 3D nanoscale structure[6-8] or controlled synthesis of highly ordered assemblies,[9] Cu-based substrate can exhibit excellent SERS enhancement effect almost on the same level as Au and Ag. This opens a gate for researchers to recognize the possibility of Cu substrate with unique structures for SERS tests.

Graphene has attracted huge amount of attentions for SERS applications in recent years due to its ability to generate stron chemical enhancement (CM). Different research systems based on graphene such as few-layer graphene solid film[10] an graphene nanocolloids[11,12] have been carried out, which show that it offers a large flat surface to adsorb molecules through π-π interactions and effective charge transfer, but graphene alone provides limited enhancement factor (EF). Combining graphen nanosheets (GNs) with metallic NPs is now a hot idea fo researchers to design and synthesize new materials with synergetic effect. Apart from the costly and equipment-dependent graphene-metallic film strategy,[13-15] two other kind hybrid structures have been developed, namely graphene decorated with metallic NPs (G-NPs) and graphene encapsulated metallic NPs (M@G NPs). Metallic NP decorated by graphene are commonly produced by wet chemical methods.[16-19] Among these approaches, however, th strong interaction between functional groups on the basal plane and metallic ions makes graphene easy to aggregate and ther may be residue of organic additives to be considered in case of disturbance in high-sensitive detection. Meanwhile there is n effective protection to the metallic NPs from possible oxidation or photo-induced reactions by direct contact with penetratin analytes.[20] As for the graphene encapsulated metallic NPs, they inherit the idea of 'shell-isolated SERS', which was proposed t inert the surface of metallic NPs by introducing an isolated stable and pin-hole free shell layer outside.[21] Unlike the decreased performance of metallic NPs encapsulated

[a] School of Materials Science and Engineering and Tianjin Key Laboratory of Composites and Functional Materials, Tianjin University, Tianjin, 300072, P. R. China. E-mail: cnhe08@tju.edu.cn; nqzhao@tju.edu.cn
[b] Collaborative Innovation Center of Chemical Science and Engineering, Tianjin 300072, China.

Electronic Supplementary Information (ESI) available: [details of any supplementary information available should be included here]. See DOI: 10.1039/x0xx00000x

traditional SERS coatings such as SiO_2,[21,22] polymers,[23,24] and amorphous carbon,[25,26] graphene shells with few layers coupled with metallic NPs serve as additional CM enhancement.[27] M@G NPs synthesized by CVD from gaseous carbon sourse[20] or electrostatic interaction[27,28] both succeeded to solve the problem of stability of metallic NPs like Cu for SERS tests. But inherent problems still remain unsolved like inadequate acceptance of the incident laser caused by poor distribution of quasi-zero dimensional M@G NPs on a flat wafer substrate. Therefore, it is of great importance to develop a novel and efficient graphene/Cu substrate material with high sensitivity and good reproducibility.

In this work, we demonstrate a nitrogen-doped graphene networks supported Cu NPs encapsulated by few-layer graphene shells (Cu@G-NGNs) as a sensing platform, which were synthesized by a simple and scalable in-situ chemical vapor deposition (CVD) technique with the assistance of a template of three-dimensional (3D) NaCl self-assembly. In the constructed architecture, a high density of Cu NPs (~20 nm) uniformly anchored on 3D interconnected nitrogen-doped graphene network can provide a large surface area for SERS tests, while the graphene shells (~1 nm thickness) around the metallic core can ensure structural stability of Cu NPs. Therefore, after the Cu@G-NGNs composites were transferred onto a glass slide to obtain a uniform 6-μm-thick film as SERS substrate, a dramatic improvement in SERS performance was achieved by detecting rhodamine 6G (R6G) and crystal violet (CV) as probe molecules. Furthermore, the results show that the prepared substrates performed with a satisfying sensitivity, reproducibility and stability. Numerical simulations based on the finite element method (FEM) theory further identified the electromagnetic enhancement of Cu@G-NGNs composite structure, in good agreement with the experimental results.

Experimental section

Materials

Cupric nitrate trihydrate ($Cu(NO_3)_2{\cdot}3H_2O$), urea ($CO(NH_2)_2$), glucose ($C_6H_{12}O_6$), sodium chloride (NaCl), α-terpineol, ethyl cellulose, ethanol and acetone were purchased from Tianjin Kemiou Chemical Reagent Co., Ltd. Rhodamine 6G (R6G) and crystal violet (CV) were obtained from Sigma-Aldrich. Cu NPs were got from Beijing Dk Nano technology Co., LTD. All of these reagents were used without further purification.

Synthesis of the Cu@G-NGNs Powders

In a typical preparation process, 0.930 g of glucose, 2.265 g of $Cu(NO_3)_2{\cdot}3H_2O$ and 36.590 g NaCl were dissolved in deionized water (111 mL) under intense stirring to obtain a homogeneous solution. Then, 0.020 g of $CO(NH_2)_2$ dissolved in 10 mL deionized water was added to the previous solution drop by drop with constant stirring. The obtained solution was frozen in a refrigerator at -20 °C for 24 h. By using a freeze-drying technology, the water from the solution was eliminated to obtain dry gel, which was then grounded to a fine composite powder as precursor. During the CVD process, 10 g of the composite powder placed in a quartz boat was annealed at 750 °C for 2 h under H_2 and then cooled rapidly (within 5 min) to room temperature under the protection of H_2. The synthesized products were washed with deionized water severa times to remove NaCl, and then pure Cu@G-NGNs (th resulting sample is also referred as Cu-20 during discussion) were obtained after drying at 80 °C in a vacuum oven. Fo comparison, 3D Cu@G-GNs was synthesized under the same fabrication process by changing the glucose weight to 0.938 g and without adding urea. Two groups of contrast tests with different Cu contents were carried out by synthesizing Cu@G-NGNs under the same process but changing the $Cu(NO_3)_2{\bullet}3H_2O$ weight to 1.132 g and 3.020 g in precursors, and the resulting samples were referred as Cu-50 and Cu-240, respectively .

Preparation of Cu@G-NGNs Painting Film

To prepare paste for painting, the resulting 3D Cu@G-NGNs powders were mixed with α-terpineol, and ethyl cellulose in ethanol solution (50 mL) under ultrasonication treatment to form a colloid with the weight ratio of 1:3:1. After evaporating of ethanol in a 70 °C water bath heating, the colloid was painted onto a clean glass slide to form a homogenous 6 μm thick film with a glass rod by sliding over the tape-covered edges, followed by drying at 120 °C for about 10 min t evaporate α-terpineol. Cu@G-NGNs painting film prepared fo SERS tests was obtained after annealing at 400 °C for 1 h in H atmosphere to remove ethyl cellulose and reduce possible copper oxides in the painting process.

Characterization

Scanning electron microscopy (SEM) images were acquired b using a Hitachi S-4800 field emission electron microscope Transmission electron microscopy (TEM) images were obtained by using a FEI Tecnai G^2 F20. Powder X-ray diffraction (XRD) patterns were obtained on a Rigaku D/max diffractometer with Cu Kα radiation at a wavelength of 1.54 Å to determine the phase composition and crystallinity. Raman spectroscopy of graphene and SERS tests were performed using a Renishaw inVia Raman Microscope. The laser spot size was 1 μm^2 and a ×50 objective (numerical aperture 0.75) was used. Thermogravimetric analysis (TGA) was carried out on the TGA/DSC (METTLER TOLEDO, Switzerland) to analyse the thermal behaviour of the powder during heating. The sample weight was 30 mg and heating was performed in a alumina crucible at a rate of 5 $°C{\cdot}min^{-1}$ up to 1000 °C. X-ray photoelectron spectroscopic (XPS) measurement of the Cu@G-NGNs was carried out on a PHI 1600 ESCA system. UV-vis absorbance and transmittance spectra were recorded with a Shimadzu UV-3600 spectrometer.

SERS Sensitivity Measurements

To ensure good molecule adsorption, the as-synthesized Cu@G-NGNs painting films on glass slides were immersed in 1 mL R6G/CV ethanol solutions (from 10^{-3} to 10^{-7} M) for 6 h, taken out and washed to remove the residues with ethanol th

dried in air. The excitation laser wavelength was 532 nm for R6G test and 633 nm for CV test. The laser power was 0.5 mW for tests to prevent samples from photo-induced damages. All the SERS spectra were acquired with the acquisition time of 10 s. The Cu NPs for SERS tests were mixed with ethanol (5 mg/mL) under ultrasonification and then spin coated on a Si/SiO_2 wafer.

Finite Element Numerical Simulation Method

To investigate the enhancement effect of electromagnetic mechanism (EM) in the unique Cu@G-NGNs composite structure, FEM numerical electromagnetic simulations were performed.[29] In the simulations, Cu NPs were reduced to hemispheres with a diameter of 20 nm (mimicking the average dimension of Cu NPs in experiments). The graphene was deformed into conformal shape to entirely contact the top surface of the bottom Cu hemisphere. A layer of flat graphene was placed under the bottom surface of Cu. A semi-infinite glass substrate was used as the substrate of the studied materials. A plane light wave was launched perpendicular to the substrate with a single, polarized electrical field, Ex. The simulation area was 80 nm × 80 nm in the horizontal dimension. Perfectly matched layer (PML) absorbing boundary conditions were applied in the boundary. The optical power absorbed in Cu hemisphere is related to the overlapped electric field and can be simply described as

$$P_{abs} = \frac{\pi c \varepsilon_0}{\lambda} \int \varepsilon''(\lambda) |E(\lambda)|^2 \, dV \qquad (1)$$

Where λ is the wavelength of incident light, c is the light speed, ε_0 is the permittivity in vacuum, $\varepsilon''(\lambda)$ is the imaginary part of the dielectric constant, $E(\lambda)$ is the electric field as a function of λ, and the integral is taken over the volume. The dielectric constant of Cu was calculated according to the Drude model.[30] The refractive index of graphene in the visible range is governed by $n_g = 3.0 + C(\lambda_0 / 3)i$, where $C \approx 5.446\ \mu m^{-1}$, and λ_0 is the vacuum wavelength. The thickness of the monolayer graphene was set as 0.5 nm.

Results and Discussion

Fig. 1 depicts the synthetic process of Cu@G-NGNs and their further painting film preparation for SERS measurements, together with illustration of the unique synthesized structure of 3D Cu@G-NGNs. Here the glucose ($C_6H_{12}O_6$) was chosen as carbon precursor due to two reasons: First of all, glucose could pyrolysis more easily into dextran, a cross-linked polymeric material with strong viscosity, at the early period of heat treatment, which is favorable for building NaCl particles into 3D self-assemblies; Secondly, the polar hydroxyl and ether oxygen groups of glucose fix Cu^{2+} through complexing action into inactive complexes, thus effectively confining Cu grains upon heating.[31] During the synthesis, cupric nitrate, glucose and NaCl were dissolved in distilled water to get a homogeneous solution, then the urea solution was dropped slowly to react with Cu^{2+} by the formula as follows:

$$Cu(NO_3)_2 + 2CO(NH_2)_2 \rightarrow [Cu(CO(NH_2)_2](NO_3)_2 \qquad (2)$$

to prevent the precipitation of Cu^{2+} into $Cu(OH)_2$. The solution was then frozen into solid state and subjected to freeze-drying. In the freeze-drying process, NaCl crystals which were face-to-face self-assembled separated from the concentrated solution, squeezing the sticky gel into homogenous coating as well as distributing the metal salt $Cu(NO_3)_2$ on the contact surface (Fig. S1 a and b). Upon heating at high temperature under H_2 (namely, the CVD process), the Cu ions were reduced to small and uniformly distributed Cu NPs confined by NaCl assemblies, which acted as catalysts for the carbonization process of the glucose chains and finally promoted the solid carbon source transferred into graphene walls (Fig. S1c and d†). In this process, the solid nitrogen source urea was pyrolyzed to N atoms and then doped into the graphene lattice. The heated powders were filtrated and dried for eliminating NaCl templates. After that, by a simple and effective painting method, a uniform 6 μm film was formed on a glass slide for SERS tests.

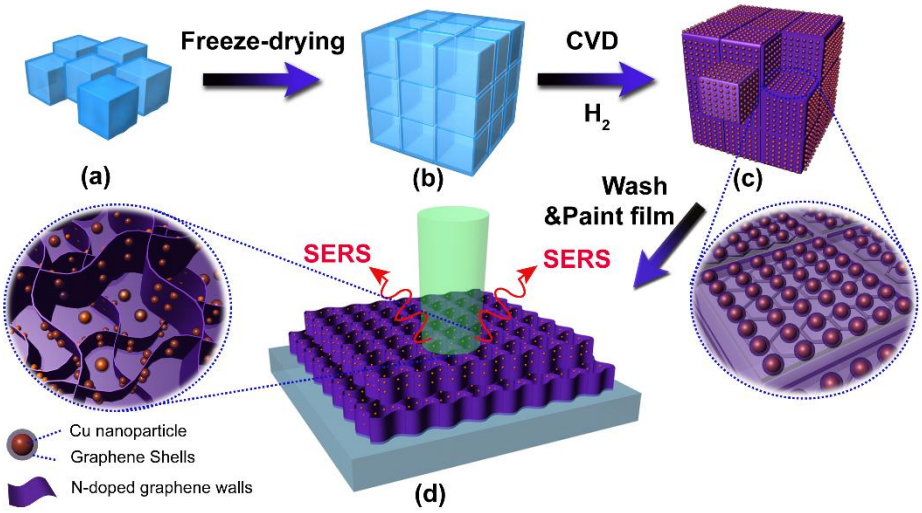

Fig. 1. Schematic illustration of the synthetic process of 3D Cu@G-NGNs and its painting film. (a) $Cu(NO_3)_2$-$C_6H_{12}O_6$-$CO(NH_2)_2$ hybrids coated NaCl in the frozen solution. (b) $Cu(NO_3)_2$-$C_6H_{12}O_6$-$CO(NH_2)_2$ coated NaCl self-assembly. (c) Cu@G-NGNs coa

NaCl self-assembly. (d) 3D Cu@G-NGNs painting film for SERS test.

The phase composition of the as-prepared product (3D Cu@G-NGNs) detected by the wide-angle XRD is displayed in Fig. 2a. For the peaks at 40−80°, the three sharp diffraction peaks at 43.3°, 50.4°, and 74.1° correspond to the reflections from the (111), (200), and (220) crystal planes of face-centered cubic (fcc) structured copper (JCPDS No. 85-1326), respectively. No obvious impurity diffraction peak was detected, confirming the high purity of the elementary Cu. To identify the composition of the Cu@G-NGNs powders, thermal gravimetric analysis (TGA) and differential scanning calorimetry (DSC) were conducted (Fig. 2b). With the strategy to oxidize Cu into CuO by heating in air, we got original content of Cu to be 79.3 wt. % by calculating the final weight of CuO. The exothermic peaks of the DSC curve at 252 °C, 291 °C and 372 °C correspond to the transformation process $Cu(s)\rightarrow Cu_2O(s)$, $Cu_2O(s)\rightarrow CuO(s)$ and $C(s)\rightarrow CO_2(g)$, respectively. The shift of exothermic peaks towards higher temperature compared to the reported Cu@G structure indicates the good thermal stability of Cu@G-NGNs.[32] The morphology of the Cu@G-NGNs was analyzed by SEM, with the results shown in Fig. 2c-e. Obviously, a 3D interconnected graphene network can be seen with a replicate of the morphology of 3D NaCl assemblies in the precursor powders (see Fig. S1a and b†). By varying the Cu contents to 67.7 wt.% and 87.3 wt.% respectively (Fig. S2), the resulting samples of Cu-50 and Cu-240 still presented the structural integrity of 3D NGNs similar to Cu-20 (Fig. S3a and b†). When investigated the SEM images of Fig. 2c-e in detail, the graphene walls displayed curled and transparent features, indicating the 3D graphene walls were of ultrathin thickness and with high mechanical flexibility. Thousands of uniform Cu@G NPs anchored on the graphene walls were observed from the high-magnification SEM images of Fig. 2d and e. The Brunauer−Emmett−Teller (BET) surface areas of 3D Cu@G-NGNs was calculated to be 79.324 m^2/g (Fig. S4†), which is larger than recently reported data of metal sponges, foams or particle assemblies (Table S1†). Also, the specific surface area of Cu@G-NGNs surpasses that of rGO/Cu NPs due to advantageous features of the 3D network structure which serves as an ideal platform for homogeneously loading ultrahigh density of Cu@G NPs.

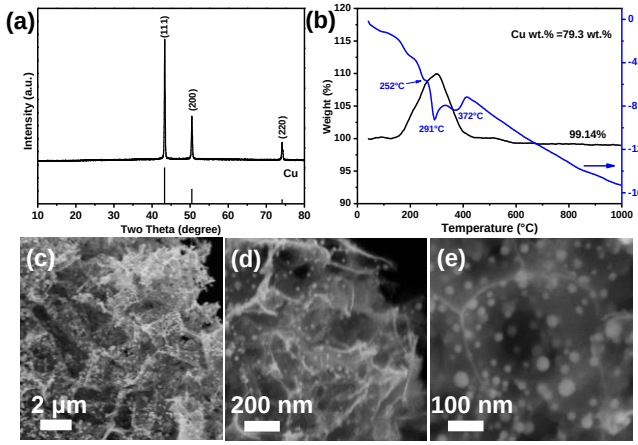

Fig. 2. (a) XRD pattern, (b) TGA and DSC profiles, and (c-e) SEM images of 3D Cu@G-NGNs composites

To obtain more detailed microstructural insight, Cu@G-NGNs were investigated by TEM and HRTEM (Fig. 3a-d). The resulting nitrogen-doped graphene networks serve as support uniformly decorated with polyhedral Cu NPs (Fig. 3a and b). The average particle size of the Cu NPs is 16.3 nm (Fig. 3e) calculated from 50 NPs, exhibiting a uniform size distribution with the standard deviation of 1.88 nm. A completely difference in size and distribution of Cu NPs can be observed for Cu-50 and Cu-240 as a result of the different Cu contents (Fig.S3c and d†). According to images of higher TEM magnification (Fig. 3c), we further identified the unique core-shell structure of Cu@G in Cu@G-NGNs. From Fig. 3c and Fig. S6†, we can see a clear graphene shell with 4 layers homogenously coated on the outside edge of the Cu core. The spacing of the adjacent lattice planes for the shell is 0.34 nm, corresponding to (002) planes of graphite, while those for the core is 0.21 nm, consistent with the (111) plane of Cu crystal. The relatively high-quality of the graphene wall is confirmed from Fig. 3d, in which a defined edge of three graphene layers can be seen. The HRTEM results correspond well with the SEM measurements, explicating the significant difference in morphology between Cu@G-NGNs with the previous reported graphene/Cu NPs hybrids.[32,33] Raman spectroscopy was used to further evaluate the characteristic and quality of the graphene in the 3D Cu@G-NGNs. To identify the influence of N-doping to the quality of graphene walls, we did a contrast test by synthesizing Cu@G-GNs (Fig. S5†) whose precursor without adding urea but using more glucose to equal the carbon content with that of Cu@G-NGNs. The representative Raman spectra of 3D Cu@G-NGNs and 3D Cu@G-GNs are shown in Fig. 3f. Both the spectra have two distinct peaks, i.e., a G band at 1596 cm^{-1} and a defect-related D band at 1336 cm^{-1}. The I_D/I_G of 3D Cu@G-GNs is 0.72, which is lower than reported data of rGO/Cu nanocomposites.[34] For nitrogen doping, the substitution of nitrogen atoms is usually accompanied by the introduction of defects into the graphene surface,[35] which accounts for the larger ratio of I_D/I_G (≈0.80) in Cu@G-NGNs than that in Cu@G-GNs. The appearance of unusually shaped 2D peaks at 2300−3200 cm^{-1} can be explained by the combined effect of planar graphene walls and nonplanar structure of graphene coating layers. To better explain the reason for the broad 2D region, they were fitted using Lorentzian profiles and plotted in the insets of Fig. 3f. The broad 2D region could be divided into the same 2D, D+G peaks at 2680 and 2951 cm^{-1}.

D+G band is correspondent to the nonplanar graphitic layers, derived from strained structure.[36]

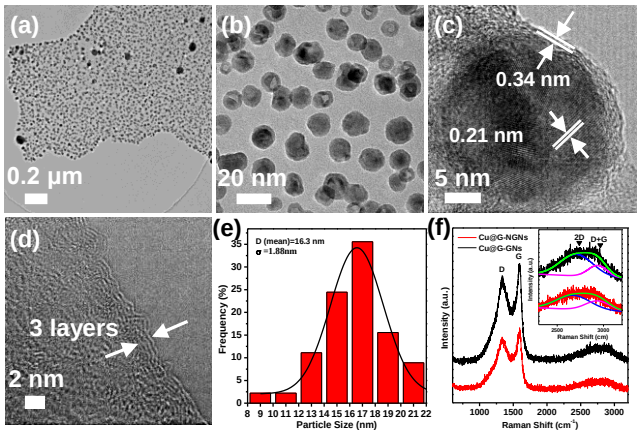

Fig. 3. (a) and (b)TEM images of Cu@G-NGNs. (c) HRTEM image of Cu@G NPs. (d) HRTEM images of the edges of N-doped graphene walls. (e) Particle size distribution of Fig. 3(b). (f) Raman spectrum of Cu@G-GNs and Cu@G-NGNs.

In order to investigate the distribution and composition of the surface state of 3D Cu@G-NGNs, energy dispersive X-ray spectroscopy (EDS), scanning transmission electron microscopy (STEM) element mapping analysis and XPS characterizations were carried out. The peaks of Cu, O and C were observed in the EDS image (Fig. S7†), and the existence of molybdenum (Mo) peek is due to the Mo grid substrate. The N element was indistinguishable as a result of the fact that the content of N is very low in comparison with the other elements and possibly small-part overlapping occurred as the position of N is very close to C and O. The relative content of N element doped in graphene from XPS analysis of Cu@G-NGNs was calculated as 1.10 at. % (see Fig. S8† and Table S3†) and the STEM element mapping result confirms that nitrogen atoms are homogenously distributed in the GNs, which proves the successful nitrogen doping in graphene materials. The high-resolution spectrum of Cu 2p (Fig. 4b) obviously shows that the binding energy peaks at 932.4 and 952.6 eV are corresponding to Cu $2p_{3/2}$ and Cu $2p_{1/2}$ photoelectron transitions, respectively, which is the characteristic of Cu in the zero-oxidation state (Cu(0)) or monovalent state (Cu (I)).[33] The small shoulder around 934.5 eV on the higher binding energy side of the Cu $2p_{3/2}$ indicates the presence of the divalent state of copper (Cu(II)) on the surface which is confirmed by the existence of Cu $2p_{3/2}$ satellite peaks at 941.9 eV and 943.7 eV.[37] To the best of our knowledge, Cu (0) and Cu (I) are hard to discriminate because they have ~0.3 eV separation for Cu $2p_{3/2}$ XPS. So Auger Cu LMM spectrum was applied to identify the existence of Cu (I) at 569.7 eV (as shown in inset of Fig. 4b).[38] The presence of Cu (II) and Cu (I) is not unusual as the size of the Cu nanoparticles are extremely small so Cu (0) in nanoparticle formed on the surface may be partially oxidized to Cu (I) or Cu (II) by atmospheric oxygen. High-resolution spectrum of N1s core level (Fig. 4c) can be deconvolved into four possible electron states: pyridinic N (398.3 eV), pyrrolic N (399.7 eV,), and low content quaternary N (402.1 eV), pyridinic-oxidized N (402.7 eV), demonstrating that nitrogen is successfully merged into the aromatic carbon nanostructure.[39] C 1s spectrum further reveals the bonding configurations among the basic carbon frameworks (Fig. 4d (a)). The major sharp peak at 284.5 eV related to the graphitic carbon (sp^2 carbon) indicates that most carbon atoms were arranged in conjugated honeycomb lattices. The broad peaks at 286.1 and 288.8 eV reflect various heteroatom–carbon configurations, related to the C-O or C-N and the C=O type bond, respectively.[3] Especially, the peak at 288.8 eV is ascribed to the physisorbed oxygen on the graphene walls, showing the evidence that N-doping caused more defects on the surface of graphene walls and in turn decreased the surface energy which is verified by a simple measuring of contact angle (insets). The contact angle between Cu@G-GNs substrate and ultrapure water reduced from 138° to 128° after mildly Nitrogen doping. The reduced surface energy helps to improve the adsorbability of heteroatoms to the surface of substrate and benefits effective contact between probe molecules and the SERS substrate.

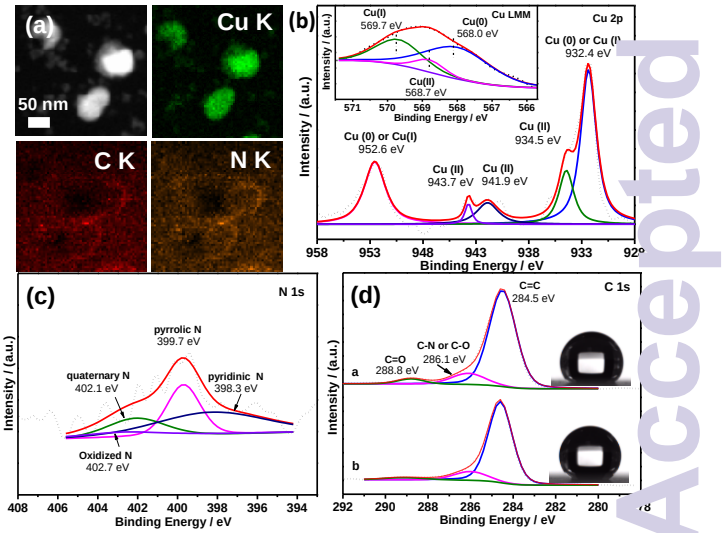

Fig. 4. a) STEM element mapping of Cu@G-NGNs. and (b-d) XPS analysis: (b) Cu 2p and Cu LMM spectroscopy (inset) of Cu@G-NGNs; (c) N 1s of Cu@G-NGNs; (d) a: C 1s of Cu@G-NGNs, b: C1s of Cu@G-GNs and the corresponding contact angle images (inset).

According to the experimental data above, we propose a combined model to illustrate the growth process of Cu@G-NGNs (Fig. 5). In our previous study,[40] we have discussed the key role of self-assembled NaCl templates in the preparation of 3D porous graphene networks. The NaCl in the precursor holds a 3D self-assembled face-contact structure which benefits to a uniform and thin layer of hybrids gel. We separate the next CVD process in H_2 atmosphere into two stages according to the two typical reactions. Stage 1 is the transformation of Cu_n clusters from $Cu(NO_3)_2$ and nitrogen-doped amorphous carbon (NAC) from hybrids gel in lower temperature CVD. The Cu nanoclusters served as catalyst for accelerating the decomposition and carbonization process

the hybrids gel. The resultant C atoms were adsorbed on the Cu_n surface and then turned to be the Cu_n/C nanoclusters. As for the volume expansion trend of NaCl crystals upon heating, the increase of internal stress contributes to an extra squeeze stress at the internal between two adjacent NaCl crystals. It not only reduced the thickness of the NAC layers but also facilitated the movement of the as-reduced small Cu_n/C nanoclusters. In Stage 2, with the raising temperature, the Cu_n clusters moved faster with increased activity and crystalized the NAC in the way of movement, which accounts for the catalytic crystallization transformation of NAC to NGNs. They finally moved close enough to form larger Cu nanoagglomerates and in turn one single Cu nanocore for reducing their high surface activity, while the carbon atoms diffused out onto the surface and form few-layer graphene shells by in-situ catalysis of Cu core under H_2.[32] Fig. S9† confirmed the pre-formed Cu@G from Cu_n/C clusters under non-equilibrium conditions without heat preservation. H_2 also contributed to accelerate the transition of Cu@G-NGNs with the role of both carrier gas and reducing reagent to eliminate additional amorphous carbon during the annealing process. The mechanism is appropriate to explain the different sizes and distributions of Cu NPs in the samples with different Cu contents. The average particle size of Cu-50 was bigger than that of Cu-20 because insufficient nucleation sites formed in hybrids gel at the beginning of the CVD process, therefore relatively more Cu_n nanoclusters aggregated into one separated Cu nanocore with a bigger particle size. While the abnormal size growth of Cu-240 may be explained by the secondary aggregation of primary Cu nanocores located close together into clusters which is the result of an increased density of nucleation sites. Thus it can be seen that, the in-situ CVD process is more controllable than the ex-situ wet chemical composite strategy to optimize the size and distributions of metallic particles on graphene.

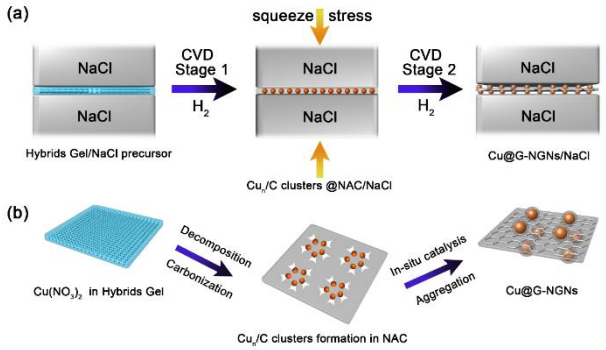

Fig. 5. The growth model and mechanism for the Cu@G-NGNs. b) is the detailed microscopic illustration of a).

The prepared Cu@G-NGNs film on a glass substrate is of great uniformity (Fig. 6a). By painting the Cu@G-NGNs into a 10 mm×10 mm film, we were able to make a facile and portable substrate for SERS tests. The film prepared by this method exhibitted a totally different morphology (Fig. 6b and c) compared to that of the previous reported rGO/NPs. As for the nature of network like structure of the Cu@G-NGNs, there is no stacking between the graphene layers nor the particle aggregation. UV-Vis spectroscopy was used to characterize the local surface plasmon resonance (LSPR) property of different nanostructured samples: Cu NPs, Cu@G-GNs and Cu@G-NGNs. As is clearly seen in Fig. 6d, the plasmonic peaks were shifted significantly with graphene introduced. The main absorption band of pure Cu NPs was located at 55[illegible] nm. A resonance shift towards longer wavelength and peak broadening of Cu@G-GNs is caused by graphene. There is no obvious difference of plasmonic peek between Cu@G-NGNs and Cu@G-GNs, confirming that the mildly nitrogen doping does not affect the plasmonic structure and contribute to the EM insignificantly. By comparing SERS tests of Cu@G-NGNs and Cu@G-GNs at the same concentration of R6G (Fig. 6e), a clear evidence of CM can be used to explain the improving intensity of the characteristic peeks. By N-doping of graphene walls and graphene shells, more probe molecules could be adsorbed on the surface area and in turn leads to more enhanced Raman scattering signals. To study the synergistic effect of Cu NPs and NGNs, we prepared two contrast samples for SERS tests. One is NGNs prepared by etching Cu NPs with marble reagents (Fig. S10 a and b†), the other is commercial Cu NPs with average diameter of 50 [illegible] (Fig. S10c†). The sample of Cu NPs was made into SERS substrate by spin coating onto a one-inch Si/SiO_2 wafer. Under the same condition with 10^{-3} M R6G, the sample of NGNs showed weaker characteristic peaks, exhibiting only a inapparent enhancement. As for the sample of Cu NPs, a high background fluorescence was observed and only peaks at 61[illegible] and 771 cm^{-1} can be detected with faintly observed intensity. A synergistic effect which combines the high EM of Cu NPs and the fluorescence quenching effect of graphene was rationally applied to account for the better enhancement of Cu@G-NGNs. Fig. 6f presents the Raman spectra of R6G under 532 nm close to the plasmonic peek. Typical fingerprint vibrational bands of R6G are significantly obvious and consistent with those reported in literature.[9] The peaks at 61[illegible], 771, 1132 cm^{-1} indicate the in-plane, out-of plane bending vibrations of C–C–C and in-plane bending vibrations of C–H, respectively. The Raman peaks of R6G symmetric modes of C–C in-plane vibrations are located at 1183, 1360, 1511, 165[illegible] cm^{-1}. As shown in Fig. 6f, the different concentrations of R6G solutions from 10^{-3} to 10^{-7} M can be detected. Even the R6G concentration decreased to 1×10^{-7} M，two minor peaks at 61[illegible] and 1183 cm^{-1} still remained clear to be seen, exhibiting strong SERS sensitivity of the substrate. Additionally, to quantitatively characterize the enhancement ability of Cu@G-NGNs substrate, we calculated the EF of the R6G molecule. The method used was described in detail in the ESI.† The EF was calculated to be 1.15×10^6 at 612 cm^{-1}, which is much higher than reported Cu substrate.[6,41,42] To further identify the SERS effect of Cu@G-NGNs, we replaced the probe molecules for crystal violet (CV). As shown in Fig. 6 g, the different concentrations of CV solutions from 1×10^{-3} to 1×10^{-7} M could be detected. Strong characteristic peaks at 803, 915, 1170, 1365, 1588 and 1614 cm^{-1} were observed from 10^{-3} to 10^{-6} M, which were in good agreement with

previously reported data.[43] A small peak at 1295 cm^{-1} was still observable for 10^{-7} M concentration. The Raman intensity shows a quasi linear increase with the increasing of the logarithm of R6G and CV concentrations (Fig. S11†), indicating that the Cu@G-NGNs substrate is a prospective platform for R6G and CV detection. Fig. S12† shows the SERS performance of Cu-50 and Cu-240 substrate using CV as probe molecules under the same test conditions. Both Cu-50 and Cu-240 could reach a concentration limit to 1×10^{-6} M, with obvious weaker intensity of characteristic lines corresponding to different concentrations. With a more uniform particle distribution and entire capsulation by graphene shells, Cu-20 is more suitable SERS substrate with optimized Cu content.

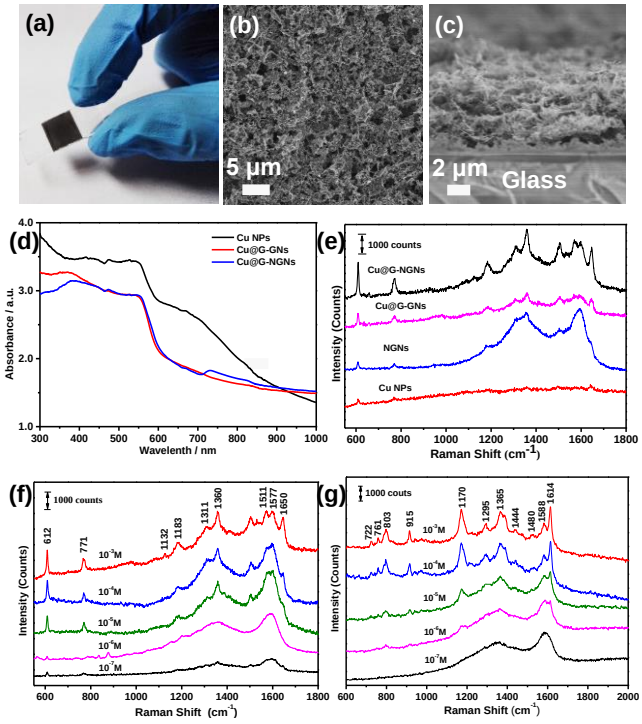

Fig. 6. (a) Digital photo of the prepared 10 mm×10 mm Cu@G-NGNs film for SERS test. SEM images of the front (b) and side(c) views of the 6-μm-thick Cu@G-NGNs film . (d) UV-vis spectra of Cu NPs, Cu@G-GNs and Cu@G-NGNs. (e) SERS spectra of 10^{-3} M R6G adsorbed on the Cu@G-NGNs, Cu@G-GNs, NGNs and bare Cu NPs, respectively. SERS spectra of R6G (f) and CV (g) at different concentrations adsorbed on Cu@G-NGNs.

The reproducibility and stability of SERS spectra are of great importance for routine applications besides sensibility. To test whether the Cu@G-NGNs film substrates were capable to give reproducible and stable SERS signals, two designed experiments were carried out based on the spot-dependent and time-dependent methods. SERS spectra of R6G molecules with a concentration of 10^{-3} M from 14 randomly selected spots on the substrate were collected for comparisons, as shown in Fig. 7a. The identical and clear peaks of R6G can be a persuasive evidence for the good uniformity of the film substrate. The time-dependent measurement was carried out on the SERS of 10^{-5} M CV on Cu@G-NGNs for 260 s, shown in Fig. 7b. It can be seen that the Raman intensity decreases very slowly with time, confirming the good stability of the prepared substrate for SERS tests.

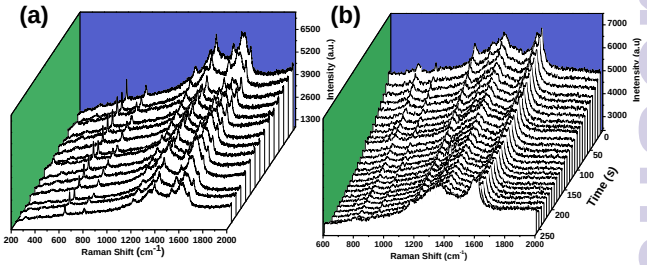

Fig. 7. (a) Reproducibility of Cu@G-NGNs film substrate i 10^{-3} M R6G. SERS spectra were collected from 14 randoml selected spots from the substrate. (b) Evolution of SER signals from 10^{-5} M CV on Cu@G-NGNs film substrate (data were collected at an interval of 10 s).

Fig. 8 a-c shows the schematics of the calculated absorption from simulation as a function of incident wavelength fo single Cu hemisphere and a single layer of graphen supporting one Cu hemisphere with or without graphen coating, respectively. The resonance wavelength for Cu-G and Cu@G-GN show a resonance shift towards long wavelength and peak broadening compared with that of the single Cu hemisphere on the substrate (Fig. 8j), in line wit the previous reported Au or Ag with graphene.[29,44] The resonance peak of Cu@G-GN shows less red-shift and narrower width than Cu-GN. The higher refractory index of graphene than air accounts for the red-shift effect and th broadening is caused by graphene ohmic loss and damping effect. We simulated electrical field intensity distributions fo the three models to study the combined effects of the coupling between graphene and Cu. From Fig. 8d-f, we can see obvious difference at the graphene-Cu interface. The two models with graphene have a more enhanced electrical field than nanoparticle model on the edge, confirming the enhancing effect of graphene. With a layer of conforma graphene coating, the electrical field close to the C hemisphere of Cu@G-GN is more localized and enhanced than Cu-GN, which is beneficial for a higher enhancemen Fig. 8 g-i show that the maximum electrical field intensit around Cu NP for Cu@G-GN structure is increased t approximately 9.4 from the value of 8 for the bare Cu NP and 8.2 for Cu loaded by monolayer graphene, corresponding to 88.36-fold enhancement of the optical absorption, compared with the 64-fold enhancement for the bare Cu NP and th 67.24-fold enhancement for the Cu loaded by monolayer graphene as estimated from formula (1). The results of th simulated electrical field verify the outstanding SERS effects of the unique Cu@G-GN structure and provide theoretic basis for the SERS tests results.

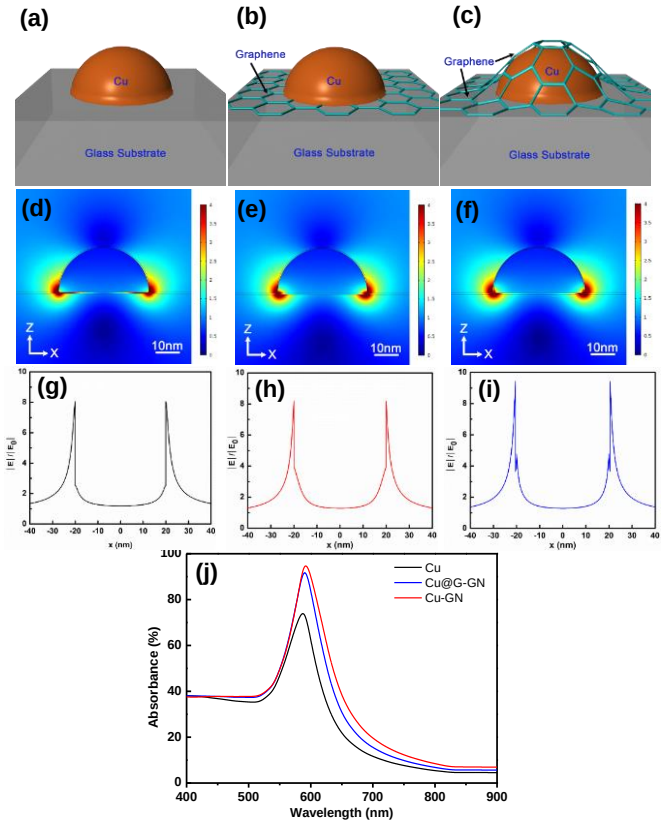

Fig. 8. (a-c) schematic of the simulated models, (d-e) FEM-simulated electric field distributions and corresponding line profiles (g-i) along the z=0.1 nm direction, (j) the simulated absorption for Cu hemisphere, graphene supported Cu hemisphere and graphene supported Cu hemisphere@G, respectively.

The results from experimental tests and FEM simulation strongly confirm that our 3D Cu@G-NGNs structure has outstanding SERS property, which can be summarized as the following aspects. First, from the plasmonic point of view, adding graphene encapsulation shells to the G-Cu system strengthens the plasmonic coupling of the nanosized Cu and graphene, therefore contributing to a greater electrical field enhancement and in turn an improved sensitivity. Second, from the construction point of view, 3D Cu@G-NGNs is the first time synthesized combining the advantages of both G-NPs and M@G NPs systems. The novel structure overcomes the limitations such as insufficient protection of G-NPs and inhomogeneous distributions of M@G NPs, thereby leading to a good reproducibility and stability. Third, from the chemical point of view, the nitrogen doping effect and the 3D supporting networks contribute greatly to the chemical enhancement.[45] The uniformly distributed nitrogen atoms bonding with carbon atoms of graphene reduce the surface energy of the substrate as well as facilitate the charge transfer between graphene layers and copper cores. With a large surface area, the supporting nitrogen doped graphene networks below Cu@G improve the absorption area of the incident laser and in turn exposure more Cu@G to the excitation. In addition, by changing parameters such as the Cu cont during the preparation process, the proper size of Cu@G an uniform distribution will be realised which are the importan factors to achieve strong near-field coupling between Cu NP Therefore, a synergetic effect was supposed to rationalize th excellent SERS effect of Cu@G-NGNs.

Conclusions

In summary, we have successfully synthesized nitrogen-doped graphene networks supported small and uniform copper nanoparticles (~20 nm) encapsulated by graphene shells structure through a one-step in-situ CVD process with the hel of self-assembled NaCl templates. Our results show that, th graphene encapsulation shells in the unique structur obviously strengthen plasmonic coupling between Cu and graphene and offer effective protection to the Cu core, w the 3D nitrogen-doped graphene networks serve as an ideal platform to uniformly anchor Cu@G and adsorb pro molecules sufficiently. As a result, the painting film substrate for SERS tests prepared by a facile but effective meth exhibits good sensibility, satisfactory reproducibility an stability. This work provides a unique composite strateg towards the design of a copper based SERS substrate Furthermore, our method is facile, green and without use complex equipment, showing a good prospect for industrial productions. We anticipate our results will benefit a furthe study on copper for SERS applications and towards more simple and cheaper SERS substrates.

Acknowledgements

The authors gratefully acknowledge the financial support b National Natural Science Funds for Excellent Young Scholar (Grant No. 51422104), National Natural Science Founda on of China (Grant No. 51272173 and No. 51472177) and Foundation for the Author of National Excellent Doctoral Dissertation of China (No. 201145), and Program for Ne Century Excellent Talents in University (NCET-12-0408).

References

1 M. Fleischmann, P.J. Hendra, A.J. McQuillan, *Chem. Phys. Lett.*, 1974, **26**, 163-166.
2 P. Zhang, Y. Sui, C. Wang, Y. Wang, G. Cui, C. Wang, F. Liu, B. Zou, *Nanoscale*, 2014, **6**, 5343-5350.
3 M. Muniz-Miranda, C. Gellini, E. Giorgetti, *J. Phys. Chem. C*, 2011, **115**, 5021-5027.
4 S.M. Angel, L.F. Katz, D.D. Archibald, L.T. Lin, D.F. Honigs, *Appl. Spectrosc.*, 1988, **42**, 1327-1331.
5 M.I. Dar, S. Sampath, S.A. Shivashankar, *J. Mater. Chem.*, 2012, **22**, 22418-22423.
6 L. Chen, J. Yu, T. Fujita, M. Chen, *Adv. Funct. Mat.*, 2009, **19**, 1221-1226.

7 Y. Tan, J. Gu, L. Xu, X. Zang, D. Liu, W. Zhang, Q. Liu, S. Zhu, H. Su, C. Feng, G. Fan, D. Zhang, *Adv. Funct. Mater.*, 2012, **22** , 1578-1585.
8 Y. Tan, J. Gu, W. Xu, Z. Chen, D. Liu, Q. Liu, D. Zhang, *ACS Appl. Mater. Inter.*, 2013, **5**, 9878-9882.
9 Q. Shao, R. Que, M. Shao, L. Cheng, S. Lee, *Adv. Funct. Mater.*, 2012, **22**, 2067-2070.
10 X. Ling, L. Xie, Y. Fang, H. Yu, H. Zhang, J. Kong, M. Dresselhaus, J. Zhang, Z. Liu, *Nano Lett.*, 2010, **10**, 553-561.
11 S. Sun, Z. Zhang, P. Wu, *ACS Appl. Mater. Inter.*, **5**, 5085−5090.
12 S. Sun, P. Wu, *Phys. Chem. Chem. Phys.*, 2011, **13**, 21116–21120.
13 W. Xu, J. Xiao, Y. Chen, Y. Chen, X. Ling, J. Zhang, *Adv. Mater.*, 2013, **25**, 928-933.
14 Y. Zhao, X. Li, Y. Du, G. Chen, Y. Qu, J. Jiang, Y. Zhu, *Nanoscale*, 2014, **6**, 11112-11120.
15 X. Li, W.C.H. Choy, X. Ren, D. Zhang, H. Lu, *Adv. Funct. Mater.*, 2014, **24**, 3114-3122.
16 Y. Zhou, X. Cheng, D. Du, J. Yang, N. Zhao, S. Ma, T. Zhong, Y. Lin, *J. Mater. Chem. C*, 2014, **2**, 6850-6858.
17 X. Tang, X. Li, Z. Cao, J. Yang, H. Wang, X. Pu, Z. Yu, *Carbon*, 2013, **59**, 93-99.
18 M. Iliut, C. Leordean, V. Canpean, C.M. Teodorescu, S. Astilean, *J. Mater. Chem. C*, 2013, **1**, 4094-4104.
19 X. Wang, G. Meng, C. Zhu, Z. Huang, Y. Qian, K. Sun, X. Zhu, *Adv. Funct. Mater.*, 2013, **23**, 5771-5777.
20 Y. Liu, Y. Hu, J. Zhang, *J. Phys. Chem. C*, 2014, **118**, 8993-8998.
21 J. Li, Y. Huang, Y. Ding, Z. Yang, S. Li, X. Zhou, F. Fan, W. Zhang, Z. Zhou, D. Wu, B. Ren, Z. Wang, Z. Tian, *Nature*, 2010, **464** ,392-395.
22 L.M. Liz-Marzán, M. Giersig, P. Mulvaney, *Langmuir*, 1996, **12**, 4329-4335.
23 M. Yang, T. Chen, W. Lau, Y. Wang, Q. Tang, Y. Yang, H. Chen, *Small*, 2009, **5**, 198-202.
24 X. Qian, X. Peng, D.O. Ansari, Q.Q. Yin-Goen, G. Chen, D. Shin, L. Yang, A. Young, M. Wang, S. Nie, *Nat. Biotechnol.*, 2007, **26**, 83-90.
25 A. Shen, L. Chen, W. Xie, J. Hu, A. Zeng, R. Richards, J. Hu, *Adv. Funct. Mater.*, 2010, **20**, 969-975.
26 X. Zhang, Z. Lu, D.H. Sim, S. Li, Y. Feng, J. Ma, H. Chen, F. Boey, H.H. Hng, Q. Yan, *Chem.-Eur. J.*, 2011, **17**, 13386-13390.
27 S. Chen, X. Li, Y. Zhao, L. Chang, J. Qi, *Carbon*, 2015, **81**, 767-772.
28 T. Kim, K. Lee, J. Choi, *Biomaterials*, 2013, **34**, 8660-8670.
29 Y. Du, Y. Zhao, Y. Qu, C. Chen, C. Chen, C. Chuang, Y. Zhu, *J. Mater. Chem. C*, 2014, **2**, 4683-4691.
30 E.D. Palik, *Handbook of Optical Constants of Solids*, Academic Press, London, 1998.
31 Y. Zhao, Z. He, Z. Yan, *Analyst*, 2012, **138**, 559-568.
32 S. Wang, X. Huang, Y. He, H. Huang, Y. Wu, L. Hou, X. Liu, T. Yang, J. Zou, B. Huang, *Carbon*, 2012, **50**, 2119-2125.
33 X. Guo, C. Hao, G. Jin, H. Zhu, X. Guo, *Angew. Chem. Int. Edit.*, 2014, **53**, 1973-1977.
34 T. Wu, M. Chen, L. Zhang, X. Xu, Y. Liu, J. Yan, Y. Wang, J. Gao, *J. Mater. Chem. A*, 2013, **1**, 7612-7621.
35 H. Wang, T. Maiyalagan, X. Wang, *ACS Catal.*, 2015, 2, 781-794.
36 S. Lee, J. Hong, J. Koo, H. Lee, S. Lee, T. Choi, H. Jung, B. Koo, J. Park, H. Kim, Y. Kim, T. Lee, *Acs Appl. Mater. Inter.*, 2013, **5**, 2432-2437.
37 P. Mondal, A. Sinha, N. Salam, A.S. Roy, N.R. Jana, S.M. Islam, *RSC Adv.*, 2013, **3**, 5615-5623.
38 P. Liu, E. Hensen, *J. Am. Chem. Soc.*, 2013, **135**, 14032−14035.
39 C. Zhang, L. Fu, N. Liu, M. Liu, Y. Wang, Z. Liu, *Adv. Mater.*, 2011, **23**, 1020-1024.
40 J. Qin, C. He, N. Zhao, Z. Wang, C. Shi, E. Liu, J. Li, *ACS Nano*, 2014, **8**, 1728-1738.
41 M. D-. Vyškovská, V. Prokopec, M. Člupek, P. Matějka, *J. Raman Spectrosc.*, 2012, **43**, 181–186.
42 H. Yang, S. He, H. Yuan, *Langmuir*, 2014, **30**, 602-610.
43 M.V. Canamares, C. Chenal, R.L. Birke, J.R, *J. Phys. Chem. C*, 2008, **112**, 20295-20300.
44 G. Xu, J. Liu, Q. Wang, R. Hui, Z. Chen, V.A. Maroni, J. Wu, *Adv. Mater.*, 2012, **24**, OP71-OP76.
45 R. Lv, Q. Li, A.R. Botello-Méndez, T. Hayashi, B. Wang, A. Berkdemir, Q. Hao, A. Elías, R. Cruz-Silva, H.R. Gutiérrez, Y. Kim, H. Muramatsu. J. Zhu, M. Endo, H. Terrones, J. C. Charlier, M. Pan, M. Terrones, *Sci. Rep.* 2012, **2**, 586.